Biomedical Signal Processing and Control 19 (2015) 1–13

Contents lists available at ScienceDirect

Biomedical Signal Processing and Control

journal homepage: www.elsevier.com/locate/bspc

Application of detector precision characteristics for the denoising of biological micrographs in the wavelet domain

Tytus Bernas[a], Roman Starosolski[b,*], Robert Wójcicki[b]

[a] Nencki Institute of Experimental Biology, Polish Academy of Sciences, Warsaw, Poland
[b] Institute of Informatics, Silesian University of Technology, Akademicka 16, 44-100 Gliwice, Poland

ARTICLE INFO

Article history:
Received 26 July 2014
Received in revised form 12 February 2015
Accepted 13 February 2015
Available online 28 March 2015

Keywords:
Microscope imaging
Biomedical imaging
Acquisition noise modeling
Wavelet image denoising
Adaptive soft thresholding

ABSTRACT

Typical fluorescence microscopy images contain large amounts of noise, which depends on the signal in a complex manner. This characteristic is substantially different from digital photography or satellite data, for which most of the existing denoising algorithms have been designed. Therefore, an efficient estimation of the noise in fluorescence micrographs and its removal pose a challenge. On the other hand, as shown previously, the use of a calibrated microscopy detector may allow computation of the signal and noise characteristics directly from the image acquisition parameters. Therefore, we propose a denoising algorithm that takes advantage of this information to obtain an estimate of the signal and the corresponding noise in the wavelet domain. This general model was constructed using actual fluorescence micrographs and utilizes intra- and inter-scale correlations of the wavelet coefficients. The signal-to-noise estimate was then applied to perform local soft thresholding in the wavelet domain. The performance of the proposed algorithm was tested using a set of images of several common subcellular structures containing various amounts of signal-dependent and signal-independent noise. The denoising performance of the new algorithm depends on the actual amount of noise and on the type of imaged structures. In every case, we demonstrated that the proposed algorithm is superior to two other locally adaptive denoising algorithms (AdaptShrink and BivarShrink) and to optimal subband adaptive soft thresholding (OraclShrink).

1. Introduction

The prominence of noise, which is caused by a low number of detected photons, is a typical problem in images registered with fluorescence microscopy. The purpose of denoising is to eliminate this random image component while retaining the biological structures under study. Traditionally, this is achieved by linear processing, such as spatial/temporal averaging and Wiener filtering. Inspired by the seminal works performed by Donoho and Johnstone [1–3], a number of studies have used nonlinear filtering based on (soft) thresholding in the wavelet domain. The main idea is to subtract the threshold value (T) from all of the coefficients greater that T and set the others to zero. In general, the threshold should be proportional to the variance of the noise and inversely proportional to the standard deviation of the distribution of the wavelet coefficients in the absence of noise [4,5]. Determination of the optimal threshold is not a trivial problem, and several methods have thus been developed to this end. The signal and noise characteristics (and thus the threshold value) may be globally estimated as proposed by the VisuShrink algorithm [1]. Another option is the adoption of subband-adaptive thresholding, as in the SureShrink algorithm [2]. Superior performance is usually achieved with another data-driven algorithm, AdaptShrink [4]. The efficiency of denoising may be further improved by taking the correlations between coefficients at different resolution scales into account [6–9].

It should be noted that the statistical models of wavelet transform coefficients adopted in these schemes were constructed for natural images [10–13]. The typical dynamic range of this type of data corresponds to 256 levels (8 bits), with the intensity histogram spanning the whole range. Conversely, when larger dynamic range is used, histograms of such images tend to be sparse [14]. This effect is a source of a significant data redundancy. Furthermore, the majority of denoising algorithms have been designed for signal-independent noise, which is the major artifact in images acquired with consumer cameras operating at a high photon flux. These prerequisites may not be met in fluorescence

* Corresponding author. Tel.: +48 322372151.
E-mail addresses: tbernas@nencki.gov.pl (T. Bernas), rstarosolski@polsl.pl (R. Starosolski), Robert.Wojcicki@polsl.pl (R. Wójcicki).

http://dx.doi.org/10.1016/j.bspc.2015.02.010
1746-8094/

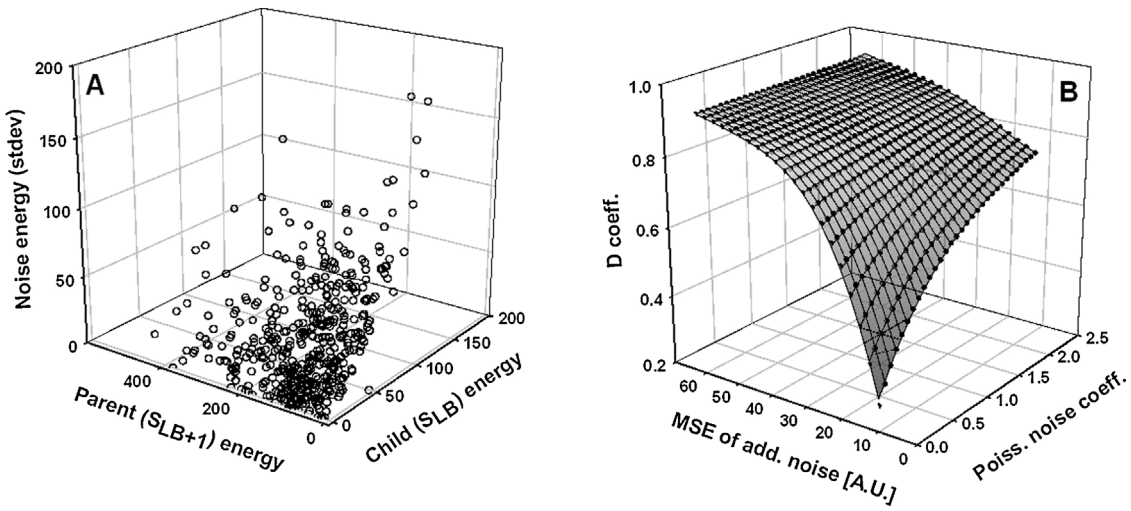

Fig. 1. Dependence of noise on the magnitude of the wavelet transform coefficients (panel A) at the first decomposition level of the HH band. One of the coefficients (C) of the signal-variance model (Eq. (3)) is represented as a function of the image registration parameters (levels of additive and Poisson noise) obtained using the Chebyshev polynomial (panel B, Eq. (4)).

microscopy, where a scarcity of light is the major limitation, but image acquisition is performed with low-noise detectors operating at a high (16 bits) dynamic range. Fortunately, when using this modality, one does not have to compute the signal and noise characteristics from the images that are to be denoised. This information may be available beforehand if a calibrated detector (e.g., CCD and PMT) is used with known image acquisition parameters [15,16].

In this study, we constructed spatial models of wavelet-domain noise as a function of the image acquisition parameters of a typical CCD detector used in microscopy. We then adapted a bivariate shrinkage algorithm [6] to compute and apply the wavelet threshold in a locally adaptive inter-scale-dependent manner. We compared the proposed denoising approach to AdaptShrink [4], the original BivarShrink [7] and optimal subband adaptive soft thresholding (OraclShrink).

2. Materials and methods

2.1. Cells and fluorescence labeling

MSU 1.1 human fibroblasts and HepG2 human hepatoma cells were cultured on 20-mm-diameter, 0.17-mm-thick coverslips placed in tissue culture Petri dishes. DMEM (Sigma), supplemented with 10% fetal bovine serum (Gibco) and antibiotics, was used. Fixed and stained bovine pulmonary artery endothelial cells were not cultured in our laboratory but purchased from Molecular Probes/Invitrogen as FluoCells prepared slide #2.

Coverslips with live cells (MSU 1.1 or HepG2) were washed three times with PBS (with Mg^{+2} and Ca^{+2}) and fixed with formaldehyde (1% in PBS at 20 °C for 1 h). MSU 1.1 cells were stained by incubation with a solution of DAPI (10 μM) for 30 min to visualize the DNA. HepG2 cells were stained by incubation with NAO

Table 1
Coefficients of the Chebyshev polynomial model (rows, Eq. (4)) corresponding to the regression coefficients of the variance model (columns, Eq. (5)) at the respective bands of the wavelet decomposition transform.

Wav. tr. band	HH			HL			LH		
Ch. cf, (Eq. (4))/R. cf (Eq. (5))	C	D	E	C	D	E	C	D	E
a	2.45E+00	8.12E−01	−4.39E−03	1.48E+01	4.74E−01	−9.14E−03	1.54E+01	4.61E−01	−1.06E−02
b	−2.36E−01	6.31E−02	1.82E−03	2.24E−01	7.03E−02	1.43E−03	2.61E−01	6.88E−02	1.62E−03
c	−7.22E−01	1.71E−01	2.27E−04	1.52E+00	2.64E−01	−6.75E−03	1.96E+00	2.62E−01	−7.95E−03
d	1.52E−02	−1.33E−02	−4.54E−04	−1.11E−01	−6.90E−03	−2.49E−04	−1.09E−01	−6.54E−03	−2.87E−04
e	2.21E−01	−9.31E−02	−9.62E−04	−1.16E+00	−6.60E−02	7.63E−04	−1.25E+00	−6.32E−02	8.98E−04
f	−5.12E−02	−5.03E−02	1.23E−03	−1.60E+00	−1.17E−02	1.68E−03	−1.64E+00	−9.75E−03	1.89E−03
g	2.12E−05	3.28E−03	1.36E−04	1.61E−02	1.29E−03	6.95E−05	1.60E−02	1.32E−03	7.07E−05
h	−2.01E−02	2.33E−02	4.30E−04	2.24E−01	8.74E−03	1.43E−04	2.34E−01	8.09E−03	1.55E−04
i	−7.74E−03	4.55E−02	−4.96E−04	7.90E−01	9.89E−03	−5.59E−04	8.06E−01	8.88E−03	−6.41E−04
j	6.94E−02	9.15E−03	−4.66E−04	2.55E−01	−1.13E−02	2.30E−04	2.29E−01	−1.13E−02	2.83E−04
k	−4.07E−05	−5.77E−04	−3.94E−05	1.81E−04	−3.42E−04	−1.62E−05	−2.34E−03	−2.82E−04	−1.43E−05
l	1.48E−03	−5.14E−03	−1.81E−04	−3.33E−02	−1.80E−03	−7.97E−05	−2.82E−02	−1.74E−03	−9.52E−05
m	1.87E−03	−1.38E−02	5.77E−06	−1.59E−01	−2.36E−03	1.21E−05	−1.56E−01	−2.19E−03	6.13E−06
n	−4.16E−02	−1.44E−02	4.53E−04	−2.46E−01	2.98E−03	5.23E−05	−2.35E−01	2.92E−03	2.50E−05
o	−2.52E−02	7.60E−04	5.15E−05	5.54E−02	3.24E−03	−1.58E−04	6.16E−02	3.05E−03	−1.81E−04
p	−6.93E−04	1.99E−04	2.33E−05	1.17E−03	8.64E−05	−2.82E−09	−7.97E−04	1.15E−04	1.71E−05
q	5.07E−05	1.47E−03	7.13E−05	1.65E−03	6.70E−04	4.26E−05	2.44E−03	6.10E−04	3.29E−05
r	1.11E−03	4.10E−03	5.34E−05	3.12E−02	8.49E−04	2.63E−05	3.18E−02	8.66E−04	8.49E−06
s	1.04E−02	6.53E−03	−1.08E−04	7.52E−02	−9.64E−05	1.50E−06	7.67E−02	−1.49E−04	−2.20E−05
t	3.16E−02	2.49E−03	−1.64E−04	2.94E−02	−1.82E−03	3.98E−05	2.24E−02	−1.58E−03	4.13E−05
u	6.03E−03	−1.09E−03	1.34E−05	−3.69E−02	−1.35E−04	3.20E−05	−3.70E−02	−4.64E−05	2.96E−05